Brazilian Journal of Geophysics, 43 (2025), 1, 1-17
Brazilian Geophysical Society
ISSN 2764-8044
DOI: 10.22564/brjg.v43i1.2336

Improving Seismic First Arrival Picking in Noisy Data: A Wavelet-Based Denoising Technique

Alireza Goudarzi*, Shadi Veisi, Seyed Hadi Dehghan-Manshadi, and Alireza Sandroos

Graduate University of Advanced Technology, Department of Earth Sciences, Kerman, Iran

*Corresponding author email: goudarzi.kgut@gmail.com

ABSTRACT. Accurate seismic first arrival picking is fundamental for geophysical interpretation and subsurface imaging. This study evaluates the performance of wavelet-based denoising techniques combined with the Translation-Invariant Shrinkage (TIS) algorithm to enhance first arrival detection. The Higher Density Discrete Wavelet Transform (HDDWT) and Double Density Wavelet Transform (DDWT) are applied to synthetic and real seismic datasets with varying noise levels. Results indicate that HDDWT outperforms DDWT in preserving critical low-frequency components and maintaining signal fidelity, particularly under high noise conditions. The P-phase Picker algorithm, when integrated with HDDWT, achieves superior accuracy and reliability in first arrival detection. These findings underscore the potential of HDDWT and TIS as robust tools for improving seismic data quality and enhancing interpretation workflows.

Keywords: P-phase Picker algorithm; Translation-Invariant Shrinkage; Double Density Wavelet Transform; Higher Density Discrete Wavelet Transform

INTRODUCTION

Accurate determination of the first arrival time of seismic waves, commonly referred to as first-break (FB) picking, is essential for characterizing subsurface discontinuities and for accurate seismic imaging. FB picking is fundamental in many geophysical applications, including seismic tomography, static correction, and velocity model building. Manual picking, although reliable in small datasets, is time-consuming, subjective, and infeasible for the increasingly large seismic datasets produced in modern surveys. Consequently, numerous automated and semi-automated FB picking methods have been developed to improve the efficiency and consistency of arrival time detection.

These FB-picking methods typically rely on detecting abrupt changes in signal characteristics such as energy, frequency content, and polarization. For example, Baer and Kradolfer (1987) introduced an automatic picking algorithm based on the short- and long-time average (STA/LTA) ratio. Murat and

Rudman (1992) and McCormack et al. (1993) incorporated neural network models to identify first arrivals in noisy traces. Fractal-based methods have also been proposed by Boschetti et al. (1996), Jiao and Moon (2000), and Gaci (2014) to detect singularities indicative of FBs. Wavelet-based arrival picking has been explored using multiscale analysis and criteria such as the Akaike Information Criterion (Zhang et al., 2003), following Chen and Stewart (2005) proposed a multi-window strategy for robust arrival detection. Other notable contributions include entropy-based and variogram fractal-dimension methods by Sabbione and Velis (2010), and phase attribute-based techniques for reflection data (Forte et al., 2016).

Filtering remains an essential preprocessing step in many picking algorithms. For example, Lomax et al. (2012) proposed FilterPicker, a robust broadband picker that incorporates filtering optimization for real-time seismic monitoring.

More recently, advanced signal processing and machine learning techniques have enhanced FB picking performance. Shang et al. (2018) applied Empirical Mode Decomposition (EMD) based denoising to improve the effectiveness of Akaike Information Criterion (AIC based) pickers. Duan and Zhang (2020) proposed a hybrid model combining classical picking and machine learning for post-correction of arrival times. Deep learning approaches have also been applied: Ayub et al. (2023) utilized hybrid Convolutional Neural Network (CNN) and Recurrent Neural Network (RNN) architectures; Yin et al. (2023) applied CNNs to large-offset data; Wang et al. (2024) introduced a graph-based approach; and Mardan et al. (2024) developed a U-Net architecture tailored for seismic data. Kim et al. (2023) proposed a method based on differences between multiwindow energy ratios to minimize the effects of noise and enhance FB picking accuracy.

Despite the diversity of FB picking algorithms, their performance remains highly sensitive to noise. Real seismic signals are often contaminated by high-amplitude noise, particularly in land environments. In such cases, denoising is not a goal in itself, but a necessary preprocessing step to enhance the performance of FB picking algorithms. Effective denoising improves signal-to-noise ratio (SNR), preserves key waveform characteristics, and ensures more accurate and robust first arrival detection.

Among the various denoising methods, wavelet domain techniques offer significant advantages due to their time-frequency localization capabilities. This study evaluates the effectiveness of wavelet-based denoising, specifically using the Higher Density Discrete Wavelet Transform (HDDWT) and Double Density Wavelet Transform (DDWT) in combination with Translation-Invariant Shrinkage (TIS) to enhance the accuracy of FB picking. Although this work does not propose a new picking algorithm, it demonstrates how advanced denoising methods can significantly improve existing pickers such as the P-phase Picker (Kalkan, 2016), particularly under challenging noise conditions.

THEORY AND METHODS

Wavelet Transform

The Fourier Transform is extensively employed in seismic processing, yet seismic data typically lacks

sparsity in the Fourier domain, as the global Fourier transform struggles to effectively distinguish local seismic data features. Consequently, various local transforms have been developed, including the short-time Fourier transform (STFT), discrete cosine transform, and wavelet transform. The wavelet transform, particularly, facilitates spatial transformation. Transferring data from time-distance to time-frequency can simplify calculations or reveal hidden information, and the transformed function may require less storage space.

In signal and image processing, wavelet theory is primarily utilized for compression and denoising purposes. By applying the Haar Discrete Wavelet Transform (HDWT) and Double Density Wavelet Transform (DDWT) to the time-frequency plane, data can be transferred for denoising purposes. Subsequently, comparing the denoising results enables the selection of the most effective transformation for data denoising (Polikar, 1996).

Higher Density Discrete Wavelet Transform

The Higher Density Discrete Wavelet Transform (HDDWT) is characterized by a set of dyadic wavelet frames with two generators. These wavelets span the time-frequency plane in a manner that offers higher sampling in both time and frequency domains. Specifically, the spectrum of the first wavelet is concentrated halfway between the spectrum of the second wavelet and the spectrum of its dilated version, denoted as $\psi_1(w)$ being concentrated between $\psi_2(w)$ and $\psi_2(2w)$. Additionally, in the frame construction, the second wavelet is translated by half-integers rather than whole-integers. The synthesis filter bank is depicted in Fig. 1 (Selesnick, 2006).

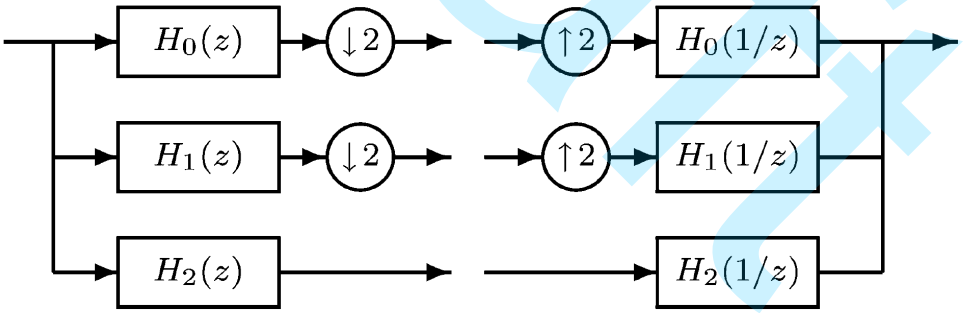

Figure 1: Schematic of the synthesis filter bank structure for the HDDWT. The first two channels are downsampled by two, while the third channel is undecimated (Selesnick, 2006).

This arrangement results in an expansive wavelet transform that exhibits approximate shift-invariance and intermediate scales. The wavelet frames are characterized by compact support and possess vanishing moments. Notably, the type of wavelet frame employed utilizes an associated filter that is bandpass rather than high-pass. Consequently, the associated sampling of the time-frequency plane differs somewhat from other transforms, as illustrated in Fig. 1. The scaling function and two wavelets are defined through the dilation and wavelet equations (Selesnick, 2006):

$$\phi(t) = \sqrt{2}\sum_{n} h_0(n)\phi(2t-n) \tag{1}$$

$$\psi_i(t) = \sqrt{2}\sum_{n} h_i(n)\phi(2t-n).\ \ i = 1.2 \tag{2}$$

When $h_i(n), n \in \mathbb{Z}$ are the filters of a digital filter bank. We consider only real-valued $h_i(n)$ of compact support. The dyadic dilations and translations of $\psi_i(t)$ form a tight frame (Selesnick, 2006):

$$\phi_k(t) = \phi(t-k) \tag{3}$$

$$\psi_{1.j.k}(t) = \psi_1(2^j t - k) \tag{4}$$

$$\psi_{2.j.k}(t) = \psi_2(2^j t - \frac{k}{2}) \tag{5}$$

If the input and output signals in Fig. 1 are x(n) and y(n), then using standard multirate identities, the Z-transform of y(n) is given by (Selesnick, 2006):

$$\begin{aligned} Y(z) = 0.5\,[H_0(z)X(z) + H_0(-z)X(-z)]\,H_0(1/z) + 0.5[H_1(z)X(z) \\ + H_1(-z)X(-z)]\,H_1(1/z) + H_2(z)H_2(1/z)\,X(z) \end{aligned} \tag{6}$$

With calculating $H_0(z)$, $H_1(z)$ and $H_2(z)$ with perfect reconstruction (PR) condition and rearranging, filters chosen (Selesnick, 2006).

Double Density Wavelet Transform

To develop the 'Ideal' double density DWT, the process begins with selecting an appropriate filter bank structure. The filter bank structure is typically illustrated in a diagram, such as Fig. 2. This diagram depicts the arrangement of filters and downsampling operations used in the double density DWT (Selesnick, 2001).

The structure described resembles the conventional two-channel filter bank utilized in implementing the critically sampled Discrete Wavelet Transform (DWT). However, in this case, the down-sampler and up-sampler in the high-pass channel have been omitted. This configuration is termed an oversampled filter bank because the combined rate of the subband signals c(n) and d(n) exceeds the input rate by a factor of 3/2 (Selesnick, 2001).

The double density DWT is subsequently implemented by iteratively applying this filter bank to the low-pass subband signal c(n). This recursive application allows for the generation of double density DWT coefficients, which capture additional detail and enable more precise analysis of the input signal. The prominent issue is the design of the filters $h_0(n)$ and $h_1(n)$ so that y(n) = x(n) (Selesnick, 2001).

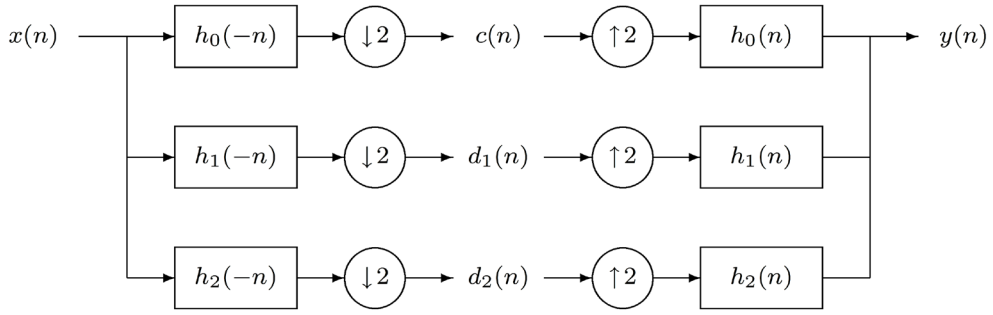

Figure 2: Diagram of analysis and synthesis filter banks used for implementing the Double Density Wavelet Transform (Selesnick, 2001).

The perfect reconstruction condition for the filter bank of Fig. 2 is derived as follows. Using basic multirate identities, we find Y (z), the Z-transform of y(n), in terms of x(z) (Selesnick, 2001):

$$Y(z) = \left[\frac{1}{2}H_0(z)H_0\left(\frac{1}{z}\right) + H_1(z)H_1\left(\frac{1}{z}\right) + H_2(z)H_2\left(\frac{1}{z}\right)\right] X(z) + \frac{1}{2}\left[H_0(z)H_0\left(-\frac{1}{z}\right)H_1(z)H_1\left(-\frac{1}{z}\right) + H_2(z)H_2\left(-\frac{1}{z}\right)\right] X(-z) \quad (7)$$

The ideal low-pass filter is:

$$H_0(e^{j\omega}) = \begin{cases} 1 & |\omega| < \pi/2 \\ 0 & \frac{\pi}{2} < |\omega| < \pi \end{cases} \quad (8)$$

For perfect reconstruction, Y (z) = X(z), it is necessary that:

$$H_0(z)H_0\left(\frac{1}{z}\right) + H_1(z)H_1\left(\frac{1}{z}\right) + H_2(z)H_2\left(\frac{1}{z}\right) = 2 \quad (9)$$

$$H_0(z)H_0\left(-\frac{1}{z}\right) + H_1(z)H_1\left(-\frac{1}{z}\right) + H_2(z)H_2\left(-\frac{1}{z}\right) = 0 \quad (10)$$

By finding answers for the perfect reconstruction condition of the filter bank of Fig. 2, we can design the filters $h_0(n)$ and $h_1(n)$ and $h_2(n)$ (Selesnick, 2001).

Translation-Invariant Shrinkage/Thresholding of Group Sparse Signals

In recent years, many algorithms grounded in sparsity principles have emerged to address tasks such as signal denoising, deconvolution, restoration, and reconstruction, among others. These algorithms frequently leverage nonlinear scalar shrinkage or thresholding functions of various forms, which have been specifically designed to achieve sparse representations of signals. Examples of such functions include the hard and soft thresholding functions, which selectively attenuate coefficients based on their

magnitudes. These functions play a pivotal role in effectively reducing noise and enhancing signal features by promoting sparsity in the signal representation (Donoho, 1995; Chen & Selesnick, 2014).

Examples of such functions are the hard and soft thresholding functions and the nonnegative garrote. Estimating x(i), i ∈ $\mathcal{I}$, from noisy observations y(i) (Chen & Selesnick, 2014):

$$\boldsymbol{y(i) = x(i) + w(i)}\,, \qquad \boldsymbol{i \in \mathcal{I}} \tag{11}$$

Where the signal x(i) is known to have a group sparse property, and w(i) is white Gaussian noise. Here, the domain of x, typically $\mathcal{I} = \{0, \ldots, N-1\}$ for one-dimensional finite-length signals. A generally effective approach for deriving shrinkage/thresholding functions is to formulate the optimization problem (Chen & Selesnick, 2014).

$$x^* = argmin_x \left\{ F(x) = \frac{1}{2}\|y - x\|_2^2 + \lambda R(x) \right\} \tag{12}$$

Where x_i , i ∈ $\mathcal{I}$ is the signal to be determined from the observation y = (y_i , i ∈ $\mathcal{I}$). The penalty function R(x) (regularizer) should be chosen to promote the known behavior of x. Many of the shrinkage/thresholding functions devised in the literature can be derived as solutions to (12), where R(x) is specifically of the separable form (Chen & Selesnick, 2014). Here, λ is the regularization parameter controlling the trade-off between data fidelity and sparsity.

$$R(x) = \sum_{i \in \mathcal{I}} r(x(i)) \tag{13}$$

For many natural (physically arising) signals, the variables (signal/coefficients) x are only sparse but do not exhibit a clustering or grouping property. The TIS algorithm acts on x as a whole without performing block-by-block processing, and minimizes the cost function (12) with the (non-separable) penalty function (Chen & Selesnick, 2014):

$$R(x) = \sum_{i \in \mathcal{I}} \left[\sum_{j \in \mathcal{J}} |x(i+j)|^2 \right]^{1/2} \tag{14}$$

The Majorization-Minimization (MM) method produces the sequence $x^{(k)}$, k ≥ 1 given by:

$$\begin{aligned} x^{(k+1)} &= arg\min_x G(x, x^{(k)}) \\ &= arg\min_x \|y - x\|_2^2 + \lambda \sum_{i \in \mathcal{I}} r(i; x^{(k)}) |x(i)|^2 \end{aligned} \tag{15}$$

Where $x^{(0)}$ is the initialization. Note that (15) is separable in x(i) , therefore, equation (15) becomes

as follows:

$$x^{(k+1)}(i) = arg\min_{x\in\mathbb{C}} \ (y(i) - x)^2 + \lambda\, r(i; x^{(k)})|x|^2 \tag{16}$$

The term $x_{i,K}^{(k)} = 0$ is undefined if $r(i; x^{(k)})$ i.e., if the i-th group is all zero. Hence, care must be taken to define an algorithm that avoids operations involving undefined quantities. Consider the following algorithm. Define $\acute{\jmath}$ as the subset of $\jmath$ where (Chen & Selesnick, 2014):

$$\jmath' \coloneqq \{i \in I : \ x^{(0)}(i) \neq 0\} \tag{17}$$

Define the update equation:

$$x^{(k+1)}(i) = \begin{cases} \dfrac{y(i)}{1 + \lambda r(i; x^{(k)})}, & i \in I' \\ 0 & i \notin I' \end{cases} \tag{18}$$

with initialization $x^{(0)} = y$. The first case of (18) is the solution to (16). The iteration (18) is the 'overlapping group shrinkage' (OGS) algorithm. The OGS algorithm produces sparse solutions by gradually reducing non-zero values of y toward zero, rather than by thresholding them directly to zero on any iteration (Chen & Selesnick, 2014).

P-phase Picker Method

Kalkan introduced an algorithm for picking P-phase arrival time in single-component ground motion acceleration or broadband velocity records, without the need for predefined detection intervals or threshold settings. The algorithm operates effectively by idealizing Single Degree Of Freedom (SDOF) oscillators with viscous (velocity-dependent) damping as moving and fixed bases. T_D is the natural period of damped vibration related to the natural period of vibration without damping (T_n) by (Kalkan, 2016):

$$T_D = {T_n}\Big/{\sqrt{1 - \alpha^{\,2}}} \tag{19}$$

The P-phase Picker operates on a digital time-series signal with a sample interval Δt. This signal can be either an acceleration record or a broadband velocity record directly output from the recorder without undergoing filtering or baseline correction. The primary objective of the P-phase Picker is to identify the onset of the P-phase by tracking the power of the damping energy. The algorithm for P-phase Picker is outlined step by step as follows (Kalkan, 2016):

1. Determine the maximum and minimum amplitudes, y_{max} and y_{min} of the power of damping energy, which will correspond to the lower and upper state levels.
2. Calculate the amplitude range yR of the power of the damping energy using $y_R = y_{max} - y_{min}$.
3. For the specified number of histogram bins (M), determine the bin width Δy as the ratio of the

amplitude range to the number of bins; Δy is found by dividing y_R by M.

4. Sort the data values into the histogram bins.

5. Identify the lowest-indexed histogram bin (i_{low}) and the highest-indexed histogram bin (i_{high}) with non-zero counts.

6. Divide the histogram into two sub-histograms. The indexes of the lower histogram bins are $i_{low} \leq i \leq \frac{1}{2} \times (i_{high} - i_{low})$ and the upper histogram bins are $i_{low} + \frac{1}{2} \times (i_{high} - i_{low}) \leq i \leq i_{high}$

7. The low-state level, which is the mode of the largest bin within the lower histogram, corresponds to the P-wave phase, and its onset is determined as the last zero crossing on the filtered seismogram before the P-wave phase arrival.

RESULTS

Check The Matching of Wavelet Transform in the PR Condition

In the first step, we examine the wavelet transforms in the perfect reconstruction (PR) condition. To achieve this, we apply wavelet transform to the signal, which yields a large number of coefficients. Subsequently, we apply wavelet transform inverse to restore the signal to its original form. To assess the PR condition, we compare the original signal with the signal obtained after applying wavelet transform and its inverse. By calculating the difference, we find that in the HDDWT domain, the difference is equal to 8.3267e^(-16), and for DDWT, it is equal to 1.1202e^(-16). This indicates that after applying both wavelet transforms to the seismic trace, the PR condition is satisfied.

The synthetic seismic data were generated using a zero-phase Ricker wavelet with the dominant frequency of 40 Hz and sampling interval of 0.002 seconds. This wavelet is ideal for its symmetric nature, ensuring that the phase does not introduce distortions in the signal.

In analyzing a synthetic, seismic noise-free trace, the performance of the Higher Density Discrete Wavelet Transform (HDDWT) combined with the Translation-Invariant Shrinkage (TIS) algorithm is superior to the Double Density Wavelet Transform (Fig. 3). DDWT-TIS suppressed the initial wavelet in Fig. 3(a), likely due to its high-pass filtering effect. HDDWT-TIS slightly altered the phase of the waveform, which must be considered when applied to signals where phase information is critical. The P-phase Picker algorithm successfully detected arrival times with minimal errors in both time domain and HDDWT cases. Power spectrum analysis (Fig. 4) revealed that HDDWT preserves all components more effectively than DDWT. In contrast, DDWT introduced signal distortions. These discrepancies, though minor, could impact the accuracy of arrival time estimation in more complex scenarios.

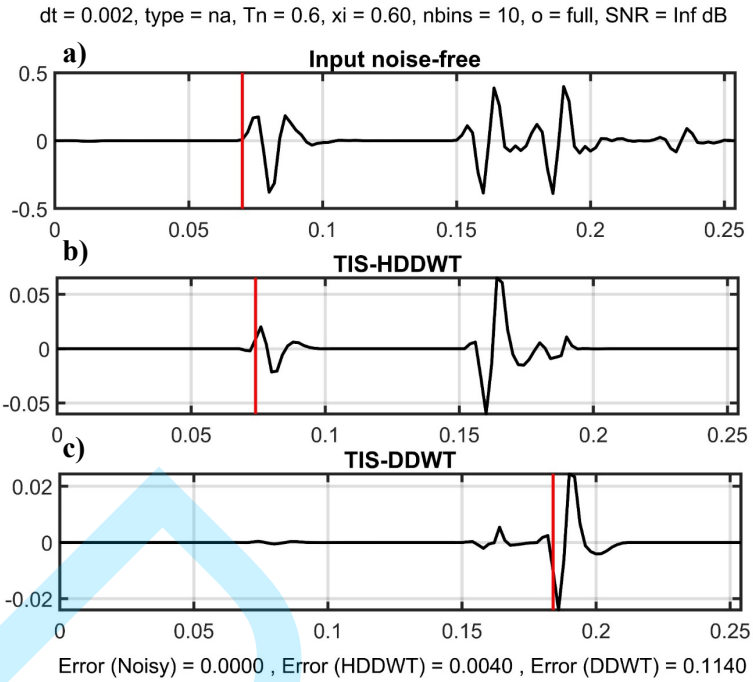

Figure 3: Synthetic seismic trace under noise-free conditions: (a) original raw trace; (b) denoised trace using HDDWT with TIS; (c) denoised trace using DDWT with TIS.

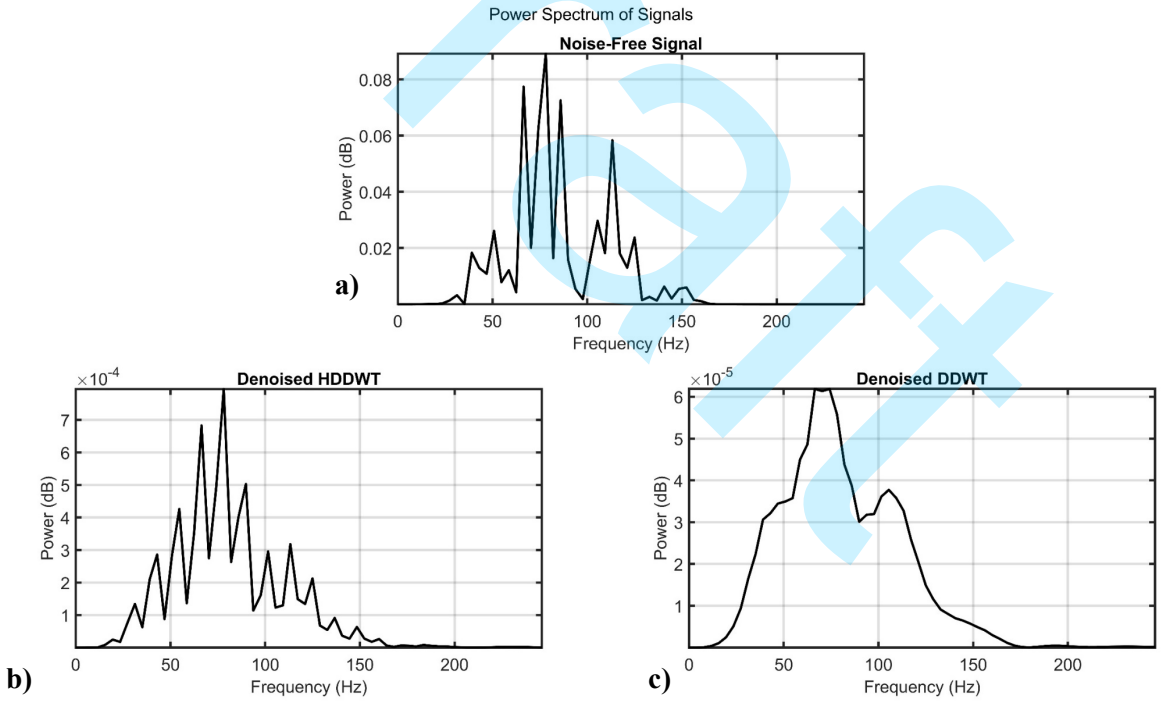

Figure 4: Power spectrum comparison of noise-free synthetic seismic data: (a) original signal, (b) HDDWT denoised signal, (c) DDWT denoised signal.

In analyzing synthetic seismic data with low noise levels (SNR ≈ 3 dB), the performance of the Higher Density Discrete Wavelet Transform (HDDWT) and Double Density Wavelet Transform (DDWT) domains combined with the Translation-Invariant Shrinkage (TIS) algorithm was compared (Fig. 5). The

P-phase Picker algorithm successfully detected arrival times with minimal errors in HDDWT, and DDWT failed. Power spectrum analysis (Fig. 6) showed that HDDWT better preserved frequency components compared to DDWT, which introduced some signal distortions. These differences might still impact the accuracy of arrival time estimation in more complex scenarios.

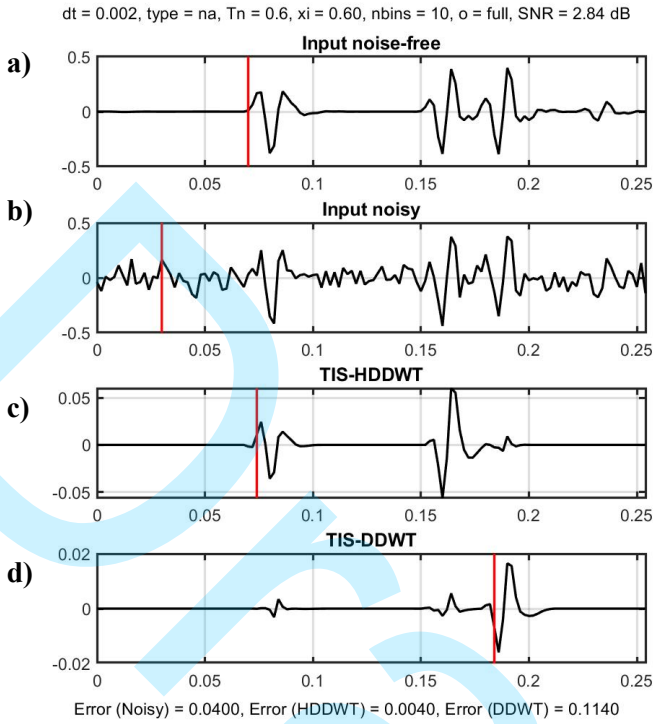

Figure 5: Synthetic seismic trace under low noise conditions (SNR = 14 dB): (a) noise-free trace, (b) noisy signal, (c) HDDWT-denoised signal using TIS, (d) DDWT-denoised signal using TIS.

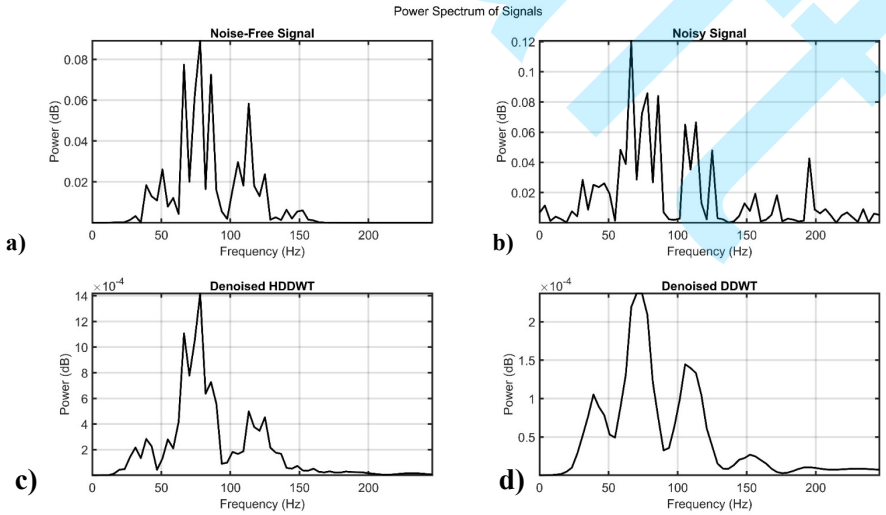

Figure 6: Synthetic seismic trace under high noise conditions (SNR = -5 dB): (a) raw noise-free trace; (b) noisy signal; (c) HDDWT-denoised signal using TIS; (d) DDWT-denoised signal using TIS.

At higher noise levels (SNR ≈ -5 dB), the HDDWT outperformed the DDWT in denoising capabilities (Fig. 7). The denoised traces from HDDWT exhibited significantly clearer waveforms. Consequently, the P-phase Picker algorithm produced smoother and more reliable first arrival picks with HDDWT. In contrast, DDWT displayed minor inconsistencies, such as jumps and drops in arrival time detection. Quantitatively, HDDWT achieved approximately 15% lower average error in first arrival picking under these challenging noise conditions, underscoring its robustness against high noise contamination. The power spectrum analysis (Fig. 8) highlighted that HDDWT preserved frequency components more effectively than DDWT.

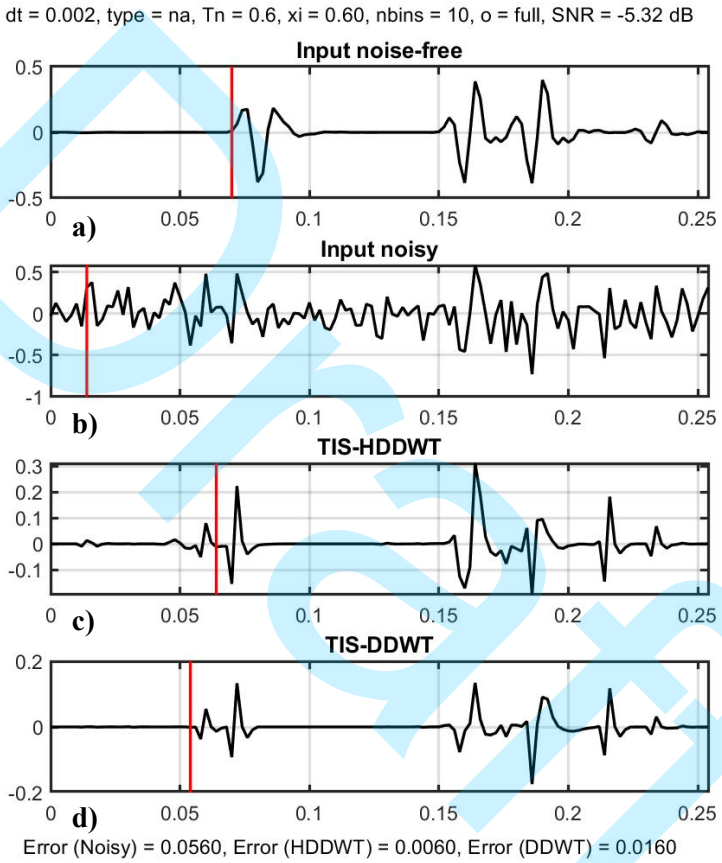

Figure 7: Power spectrum comparison of synthetic seismic trace under high noise conditions (SNR = -5 dB): original signal, HDDWT-denoised signal, and DDWT-denoised signal.

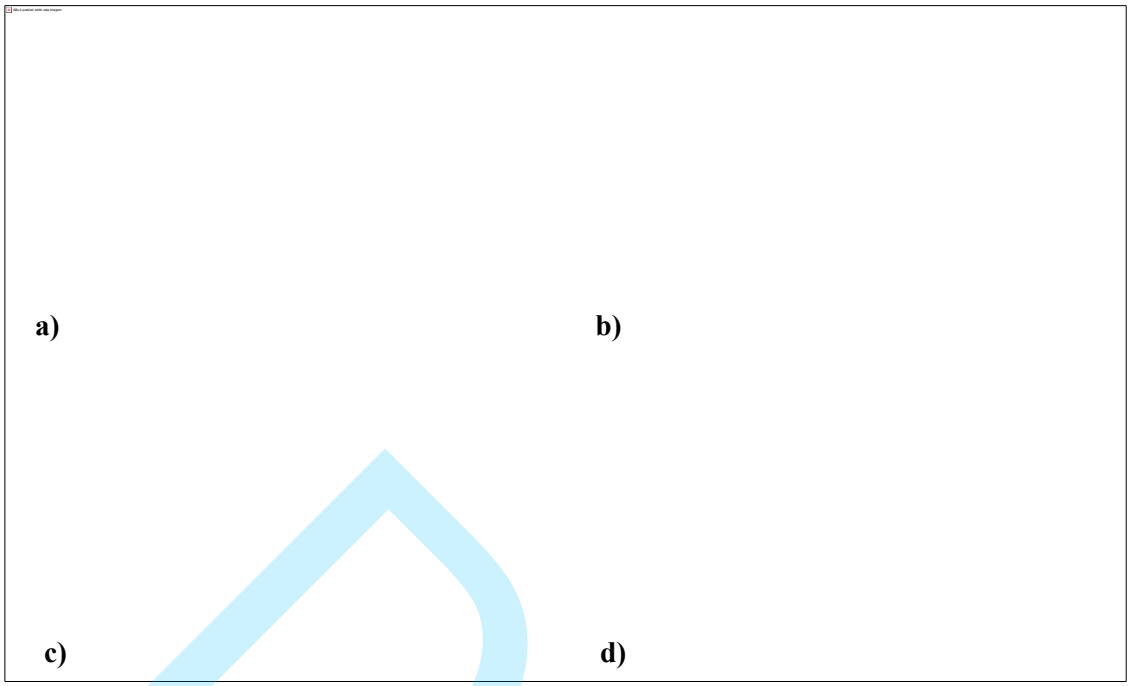

Figure 8: Power spectrum comparison for a real seismic trace: original signal, HDDWT-denoised signal, and DDWT-denoised signal.

The results presented in Table 1 summarize the performance of HDDWT and DDWT across various input SNR levels in terms of output SNR and runtime. At an input SNR level of -5 dB, HDDWT significantly outperforms DDWT, achieving an output SNR of 1.038 dB compared to 0.767 dB for DDWT. This trend of superior performance by HDDWT is consistent across all noise levels, with HDDWT consistently producing higher output SNR values. For example, at an input SNR of -3 dB, HDDWT achieves an output SNR of 3.407 dB, compared to 1.250 dB for DDWT.

Runtime comparisons indicate that HDDWT is slightly faster than DDWT for all tested noise levels. For instance, at an input SNR of -5 dB, the runtime for HDDWT is 0.000761 seconds, while DDWT requires 0.000781 seconds. Similarly, at -3 dB, HDDWT completes the operation in 0.001029 seconds, compared to 0.001141 seconds for DDWT. This demonstrates HDDWT's computational efficiency alongside its better denoising performance.

The results indicate that HDDWT achieves higher output SNR and faster runtime than DDWT across all noise levels.

Table 1. Performance comparison of HDDWT and DDWT in terms of output SNR (in dB) and runtime (in s) across various input SNR levels.

SNR(dB)	Output_SNR_HDDWT_dB	Output_SNR_DDWT_dB	Runtime_HDDWT_s	Runtime_DDWT_s
-5	1.03828	0.767349	0.000761	0.000781
-4	0.784829	0.253156	0.000616	0.000677
-3	3.40684	1.25028	0.00103	0.001141
-2	2.27892	0.62884	0.0006	0.00066
-1	0.854280	0.35056	0.00057	0.00065

A closer examination of the real seismic traces (Figures 9 and 10) highlight the challenges posed by real data high noise levels. This trace typically experiences significant noise contamination in both low- and high-frequency bands. By applying HDDWT with TIS, the traces retained critical reflection and refraction signals, ensuring that key geological features remained interpretable. In contrast, DDWT reduced noise effectively but introduced artifacts that could potentially mask weak seismic events or misrepresent the true subsurface structure. Both HDDWT and DDWT introduced distortion in the high noise case, although HDDWT retained more waveform shape than DDWT.

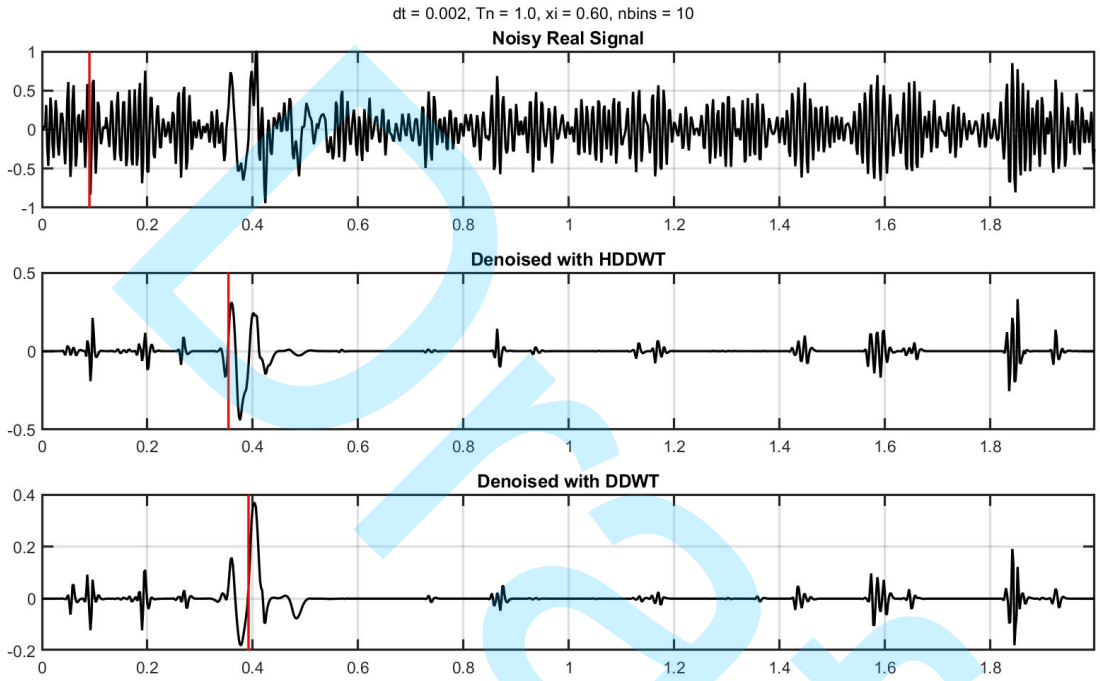

Figure 9: First arrival picks on a real seismic trace, showing results obtained from HDDWT and DDWT denoising.

Figure 10: Power spectrum comparison for a real seismic trace: original signal, HDDWT-denoised signal, and DDWT-denoised signal.

Additionally, real seismic data presented an opportunity to test the robustness of the P-phase Picker algorithm. When applied to HDDWT-denoised traces, the algorithm consistently identified the first arrival picks with higher precision, even under severe noise conditions. DDWT-denoised traces, while sufficient in many scenarios, exhibited a higher rate of discrepancies in pick locations, particularly for traces near the edges of the seismic section. The findings suggest that HDDWT, due to its superior preservation of signal integrity, offers a more reliable foundation for automated picking algorithms in real seismic data processing workflows.

A final evaluation was conducted by applying both methods to a full seismic section with 112 traces under high noise conditions (Fig. 11). The HDDWT approach demonstrated its ability to consistently suppress noise across all traces while maintaining coherent reflection patterns. This facilitated the identification of continuous horizons and improved the reliability of first arrival picking across the section. DDWT, while still functional, introduced minor inconsistencies in the continuity of reflections, which could complicate interpretation in more detailed analyses.

Figure 11: First arrival picking results on a full seismic section under high noise conditions, comparing HDDWT and DDWT denoising performance

Discussion

The findings of this study highlight the effectiveness of wavelet-based denoising methods, particularly when using TIS in the HDDWT and DDWT domains, for enhancing the accuracy of automatic first arrival picking algorithms such as the P-phase Picker. For synthetic data, HDDWT

demonstrated a consistently robust performance across different noise levels, resulting in lower error rates for first arrival picking. DDWT, while effective under low noise conditions, exhibited notable signal distortions under high noise scenarios.

For real seismic data, HDDWT outperformed DDWT in both denoising effectiveness and P-phase arrival picking accuracy. This superiority can be attributed to HDDWT's ability to preserve low-frequency components critical for seismic interpretation. Both methods demonstrated their efficacy in reducing high-frequency noise; however, HDDWT retained more energy in the low-frequency bands, ensuring higher fidelity in the reconstructed signals. The visual clarity of HDDWT-denoised traces further facilitated manual verification of first arrivals, adding a layer of practical reliability.

The computational efficiency of HDDWT further strengthens its case for use in large-scale seismic processing. Its simpler filter structure not only reduced processing time but also minimized memory usage, making it highly suitable for real-time applications. Conversely, DDWT, while computationally more demanding, remains a viable option for low noise datasets or scenarios where signal distortion is less critical.

The Translation-Invariant Shrinkage (TIS) algorithm is a powerful denoising technique used in conjunction with wavelet transforms to suppress noise while preserving critical signal components. TIS addresses the limitations of traditional thresholding methods by eliminating artifacts caused by shifts in the input signal. This is achieved by averaging the results of multiple wavelet transforms, each applied to a shifted version of the signal. The shift-invariant property ensures that denoising performance is robust across varying noise levels and signal complexities. TIS is particularly effective in handling high-frequency noise contamination, making it an ideal choice for seismic data where maintaining the fidelity of first arrivals and other critical features is essential. By leveraging TIS in both HDDWT and DDWT domains, this study demonstrates significant improvements in denoising performance and P-phase picking accuracy under diverse noise conditions.

The robustness of the P-phase Picker algorithm arises from its methodological design, which prioritizes energy-based signal detection and preprocessing techniques rather than relying strictly on the phase characteristics of the wavelet. This approach enhances its performance across a wide range of signal-to-noise ratios and waveform complexities. This adaptability allows it to function effectively with minimum-phase real seismic data, provided the signal quality is adequate and preprocessing is properly tuned.

Future research could explore the integration of machine learning techniques with wavelet-based denoising methods to further enhance their performance. Comparative studies involving other advanced denoising algorithms, such as deep learning models, could provide a comprehensive understanding of the strengths and limitations of wavelet-based approaches. Additionally, investigating the impact of varying wavelet parameters, such as filter length and decomposition levels, could yield valuable insights for optimizing wavelet domain selection.

CONCLUSION

This study demonstrates the effectiveness of wavelet-based denoising methods, particularly the HDDWT combined with the TIS algorithm, in enhancing the accuracy of seismic first arrival picking. The HDDWT consistently achieved better noise suppression and signal preservation than DDWT across synthetic and real seismic datasets. It preserved low-frequency components critical for subsurface imaging, facilitating accurate P-phase arrival picking even under challenging noise conditions. Additionally, HDDWT exhibited faster runtime, highlighting its suitability for real-time seismic applications. These advantages make HDDWT a preferred choice for improving first arrival picking accuracy in automated workflows. Future research should explore the integration of machine learning wavelet-based approaches to further enhance performance and adaptability to complex seismic scenarios.

REFERENCES

Ayub, M., & Kaka, S. I. (2023). Enhanced first-break picking using hybrid convolutional neural network and recurrent neural networks. IEEE Transactions on Geoscience and Remote Sensing, 62, 1–16. https://doi.org/10.1109/tgrs.2023.3338091

Baer, M., & Kradolfer, U. (1987). An automatic phase picker for local and teleseismic events. Bulletin of the Seismological Society of America, 77(4), 1437–1445. https://doi.org/10.1785/bssa0770041437

Boschetti, F., Dentith, M. D., & List, R. D. (1996). A fractal-based algorithm for detecting first arrivals on seismic traces. Geophysics, 61(4), 1095–1102. https://doi.org/10.1190/1.1444030

Chen, P. Y., & Selesnick, I. W. (2014). Translation-invariant shrinkage/thresholding of group sparse signals. Signal Processing, 94, 476–489. https://doi.org/10.1016/j.sigpro.2013.06.011

Chen, Z., & Stewart, R. (2005). Multi-window algorithm for detecting seismic first arrivals. In Abstracts, CSEG National Convention (pp. 355–358). https://doi.org/10.1190/1.2147921

Donoho, D. L. (1995). De-noising by soft-thresholding, IEEE Transactions on Information Theory, 41(3), 613-627. doi: 10.1109/18.382009.

Duan, X., & Zhang, J. (2020). Multitrace first-break picking using an integrated seismic and machine learning method. Geophysics, 85(4), 269–277. https://doi.org/10.1190/geo2019-0422.1

Forte, E., Dossi, M., Pipan, M., & Del Ben, A. (2016). Automated phase attribute-based picking applied to reflection seismics. Geophysics, 81(2), 141–150. https://doi.org/10.1190/geo2015-0333.1

Gaci, S. (2014). The use of wavelet-based denoising techniques to enhance the first-arrival picking on seismic traces. IEEE Transactions on Geoscience and Remote Sensing, 52(8), 4558–4563. https://doi.org/10.1109/tgrs.2013.2282422

Jiao, L., & Moon, W. M. (2000). Detection of seismic refraction signals using a variance fractal dimension technique. Geophysics, 65(1), 286–292. https://doi.org/10.1190/1.1444719

Kalkan, E. (2016). An automatic P-phase arrival-time picker. Bulletin of the Seismological Society of America, 106(3), 971–986. https://doi.org/10.1785/0120150111

Kim, D., Joo, Y., & Byun, J. (2023). First-break picking method based on the difference between

multiwindow energy ratios. IEEE Transactions on Geoscience and Remote Sensing, 61, 1–10. https://doi.org/10.1109/tgrs.2023.3255261

Lomax, A., Satriano, C., & Vassallo, M. (2012). Automatic picker developments and optimization: FilterPicker—A robust, broadband picker for real-time seismic monitoring and earthquake early warning. Seismological Research Letters, 83(3), 531–540. https://doi.org/10.1785/gssrl.83.3.531

Mardan, A., Blouin, M., Fabien-Ouellet, G., Giroux, B., Vergniault, C., & Gendreau, J. (2024). A fine-tuning workflow for automatic first-break picking with deep learning. 22, 539–552. https://doi.org/10.1002/nsg.12316

McCormack, M. D., Zaucha, D. E., & Dushek, D. W. (1993). First-break refraction event picking and seismic data trace editing using neural networks. Geophysics, 58(1), 67–78. https://doi.org/10.1190/1.1443352

Murat, M. E., & Rudman, A. J. (1992). Automated first arrival picking: A neural network approach. Geophysical Prospecting, 40(6), 587–604. https://doi.org/10.1111/j.1365-2478.1992.tb00543.x

Polikar, R. (1996). The wavelet tutorial. IOWA State University, USA, 25–60.

Sabbione, J. I., & Velis, D. (2010). Automatic first-breaks picking: New strategies and algorithms. Geophysics, 75(4), 67–76. https://doi.org/10.1190/1.3463703

Selesnick, I. W. (2001). The Double Density DWT. In Wavelets in Signal and Image Analysis (pp. 39–66). Springer Netherlands. https://doi.org/10.1007/978-94-015-9715-9_2

Selesnick, I. W. (2006). A higher density discrete wavelet transform. IEEE Transactions on Signal Processing, 54(8), 3039–3048. https://doi.org/10.1109/tsp.2006.875388

Shang, X., Li, X., Morales-Esteban, A., & Dong, L. (2018). Enhancing micro-seismic P-phase arrival picking: EMD-cosine function-based denoising with an application to the AIC picker. Journal of Applied Geophysics, 150, 325–337. https://doi.org/10.1016/j.jappgeo.2017.09.012

Wang, H., Long, L., Zhang, J., Wei, X., Zhang, C., & Guo, Z. (2024). Seismic first break picking in a higher dimension using deep graph learning. Geophysics, 89, 3, U53–U70. https://doi.org/10.48550/arXiv.2404.08408.

Yin, Y., Han, L., Zhang, P., Lu, Z., & Shang, X. (2023). First-break picking of large-offset seismic data based on CNNs with weighted data. Remote Sensing, 15(2), 356. https://doi.org/10.3390/rs15020356

Zhang, H., Thurber, C., & Rowe, C. (2003). Automatic P-wave arrival detection and picking with multiscale wavelet analysis for single-component recordings. Bulletin of the Seismological Society of America, 93(5), 1904–1912. https://doi.org/10.1785/0120020241.

Goudarzi, A: Conceptualization, Methodology, Supervision, Writing – Review & Editing; **Veisi, S.**: Investigation, Data Curation, Writing – Original Draft, Visualization; **Sandroos, A.**: Software, Formal Analysis, Validation, Visualization; **Dehghan-Manshadi, S. H.**: Resources, Writing – Review & Editing.